8×8 Ka-Band Dual-Polarized Array Antenna based on Gap Waveguide Technology

Miguel Ferrando-Rocher, *Student Member, IEEE,* Jose I. Herranz-Herruzo, *Member, IEEE,* Alejandro Valero-Nogueira, *Senior Member, IEEE,* Bernardo Bernardo-Clemente, Ashraf Uz Zaman, *Member, IEEE,* and Jian Yang, *Senior Member, IEEE*

***Abstract*—This paper describes an 8×8 fully-metallic high-efficiency dual-polarized array antenna working at Ka-band, based on Gap Waveguide concept. The radiating element is a circular aperture backed by two stacked cylindrical cavities, which are fed orthogonally to achieve a dual-polarized performance. Both feeding layers consist of a gap waveguide corporate network to reach all the cavities backing each radiating element. Cavities are naturally integrated within the bed of nails hosting grooves and ridges for guiding EM field, leading to a low-profile dual-polarized array in Ka-band. Experimental results present good agreement with simulations. Measured radiation patterns agree well with simulation and the antenna provides an average gain over 27 dBi within its operating bandwidth (29.5 to 31 GHz).**

***Index Terms*—Gap Waveguide, Ka-band, Groove Gap Waveguide, Ridge Gap Waveguide, Dual-Polarization, Array, SATCOM**

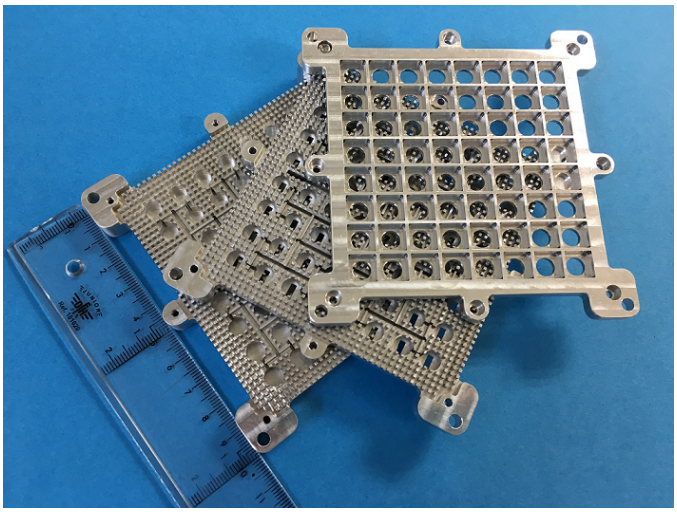

Fig. 1: Manufactured 8×8 Dual-Polarized Array Antenna based on Gap Waveguide.

I. Introduction

Broadband multimedia satellite services were initially deployed in the Ku-band using wide-beam antennas to cover large territories [1]. Today, the continuous demand for higher throughput in modern communication systems is pushing the satellite communications (SATCOM) to higher operating frequencies such as the recently developed Ka-band High Throughput Satellites (Ka-HTS). More spectrum is available in Ka-band compared to Ku-band, and additionally, Ka-satellites mostly provide spot-beam coverage allowing frequency reuse operation [2]. For above reasons, Ka-band is drawing more and more attention, especially for on-the-move communications.

Recent years have seen an intensive research effort to find compact, lightweight, and cost-effective antenna solutions for Ka-band SATCOM on-the-move applications. However, high-efficiency solutions enjoying dual-band operation, dually-polarized, low profile and low cost features, appropriate for Ka-band satellite communications, are still scarce. Among those needs, a particularly appealing one is the dual-polarized planar feature.

Utilizing two orthogonal polarizations is a widely used technique in SATCOM to provide additional spectrum in a given geographical region [3]. In that case, dual-polarized antennas allow to save costs and space, compared to the scheme where one dedicated antenna is used to each polarization.

Many dual-polarized antennas in the literature are based on microstrip-patch technology [4]-[6], thanks to their desirable features as low profile, lightweight and low cost. However, there is a big obstacle for them to be used for mm-wave band due to their huge losses for large arrays. Conversely, notable efforts have been made in the past to achieve dual-polarized antennas using other solutions, such as parabolic reflectors [7]-[8], reflectarrays [9]-[11], lenses [12]-[13], waveguide arrays [14]-[15], planar structures [16] or leaky-wave antennas [17]. These type of antennas are widely developed and studied, and they can meet some of the SATCOM on-the-move requirements.

In fact, the last two examples of waveguide arrays are remarkable for several reasons. First of all, the dual-polarized antenna in [14] is a fully metallic array providing high efficiency. Its biggest drawback is probably the use of diffusion bonding manufacturing technique, requiring great precision and cost. On the other hand, the contribution in [15] presents some similarities with the one presented here. The distribution network used, however, is quite complex, since the out-of-phase condition of E-plane splitters must be compensated. As a consequence, radiating elements are forced to be spaced $1.25\lambda_0$. In this paper, a more compact and simple corporate-

This work was supported by the Spanish Ministry of Science, Innovation and Universities (Ministerio de Ciencia, Innovacion y Universidades) under projects TEC2013-47360-C3-3-P and TEC2016-79700-C2-1-R.

M. Ferrando-Rocher, J. I. Herranz-Herruzo, A. Valero-Nogueira, and B. Bernardo-Clemente are with the Instituto de Telecomunicaciones y Aplicaciones Multimedia (ITEAM) of the Universitat Politècnica de València, c/ Cami de Vera s/n, 46022 Valencia, Spain (e-mail: miferroc@iteam.upv.es)

A. Uz Zaman, and J. Yang are with the Electrical Engineering Department at Chalmers University of Technology, Gothenburg, Sweden

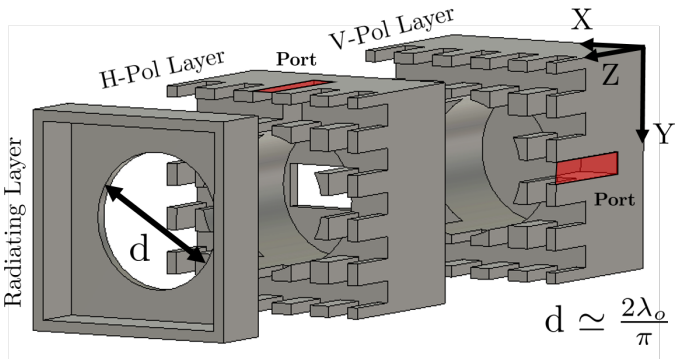

Fig. 2: Perspective exploded view of the stacked configuration of the readiating element.

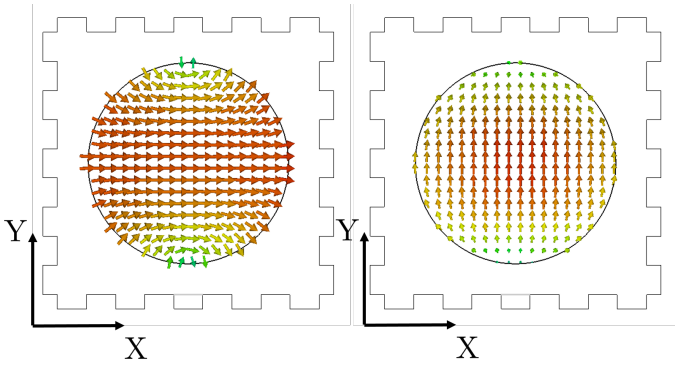

Fig. 3: (Left) E-field and (right) H-field across the radiating circular aperture at 30 GHz.

feed network is employed. The network allows to locate the apertures noticeably closer to each other (λ_0 at 30 GHz). In addition, gap waveguide (GW) technology is adopted, whose contactless capability ensures the confinement of the field even if there is no perfect electrical contact between waveguide blocks [18].

Shortly, the gap waveguide is built up of two unconnected plates: a textured surface composed by a bed of nails and a flat metal surface. The first one behaves as a high-impedance surface, thus forbidding any wave propagation as long as the distance to the opposite flat plate is less than a quarter-wavelength. Only when a groove or a ridge is inserted among the nails, wave propagation takes place [19].

Till now, several gap waveguide based low loss planar high gain antennas have been designed at mm-wave frequency range [20]-[21]. However, most of the antennas designed so far based on gap waveguide technology are linear polarized.

Making use of the benefits of this technology, an 8×8 full-metal dual-polarized array antenna (Fig. 1), especially appealing for SATCOM terminals, is presented next. It is worth mentioning that a very preliminary approach of a 2×2 dual-polarized array antenna was proposed in [22]. This paper describes a much more evolved version of that concept.

The paper is organized as follows. In Section II, the geometry and design of the radiating elements are presented. The description of the full antenna, the simulated performance as well as the design of the input ports are detailed in Section III. Section IV presents the manufacturing process and the experimental results of the fabricated array. Finally, conclusions are drawn in section V.

II. Radiating Element

The radiating elements consist of circular apertures of diameter d, which are excited by side-fed stacked cylindrical cavities. Fig. 2 shows the basic model of the radiating element. It can be seen as an open circular waveguide fed at one of its sides. Note that the cylinder could also be fed from the back, but the employed lateral feeding is more convenient for a stacked configuration.

The first approach to this type of cavities was presented in [23] to implement a circularly-polarized array antenna. Now, to conceive a dual-polarized antenna, an additional layer is

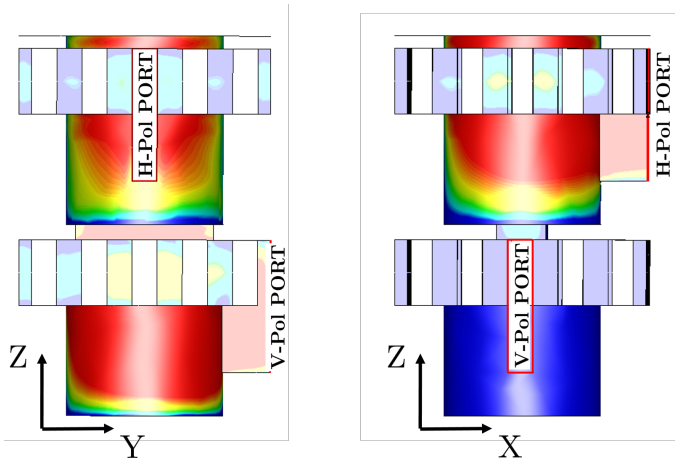

Fig. 4: E-field component in YZ and XZ planes for the radiating element based on a open cavity, when the bottom port (left) or the top port (right) is excited at 30 GHz.

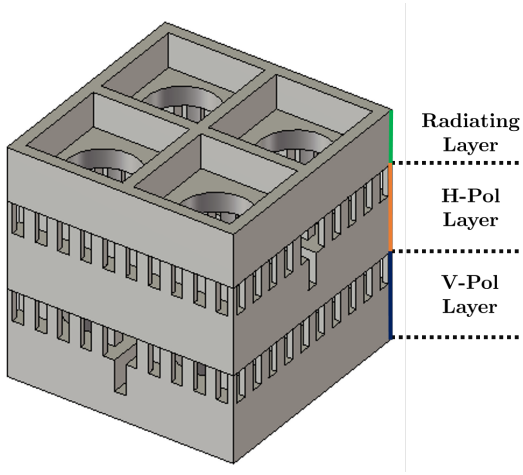

Fig. 5: 2×2 dual-polarized unit cell.

added. An orthogonal feeding scheme to the cylindrical cavity enables radiate the corresponding orthogonal linear polarized EM field to radiate. This orthogonal feeding is implemented at different heights (see Fig. 2) to be able to accommodate an independent corporate feeding network for each polarization. The upper cavity excites the horizontal polarization on the

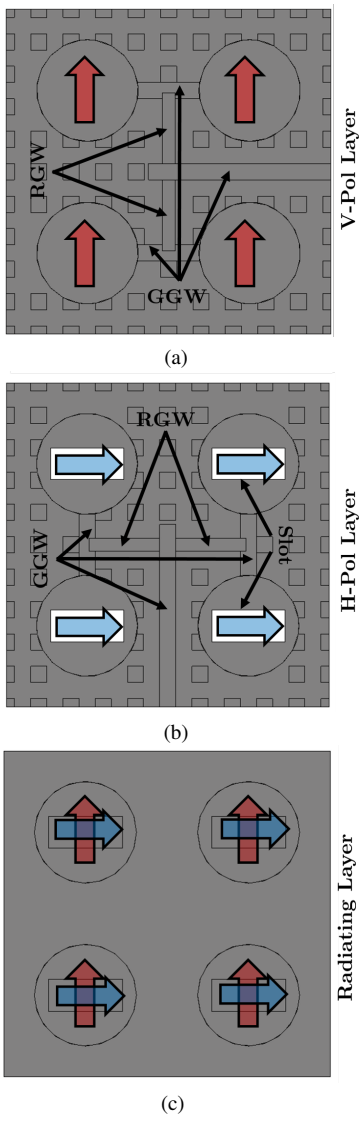

Fig. 6: Layers of the dual-polarized unit cell from bottom to top.

aperture (H-Pol) while the lower cavity allows to radiate with the orthogonal one (V-Pol). A slot is added to the floor of the upper cavity to improve the isolation between polarization.

Fig. 3 shows the electric and magnetic fields on the radiating circular aperture when one port is excited. The well-known fundamental mode of a circular waveguide is observed. In Fig. 4 the amplitude of the E-field within the cavity is represented along two cuts corresponding to the YZ and XZ planes. In this case, each subfigure corresponds to the excitation of one different port. The colored graphs show how the electric field is coupled from the input port to the radiating circular aperture. As can be also seen, the coupling between the V-Pol layer and the H-Pol layer is negligible and a good isolation between both ports is expected.

A. 2×2 Dual-Polarized Unit Cell

The 2×2 dual-polarized unit cell is shown in Fig. 5, while Fig. 6 shows the different layers of the subarray from a

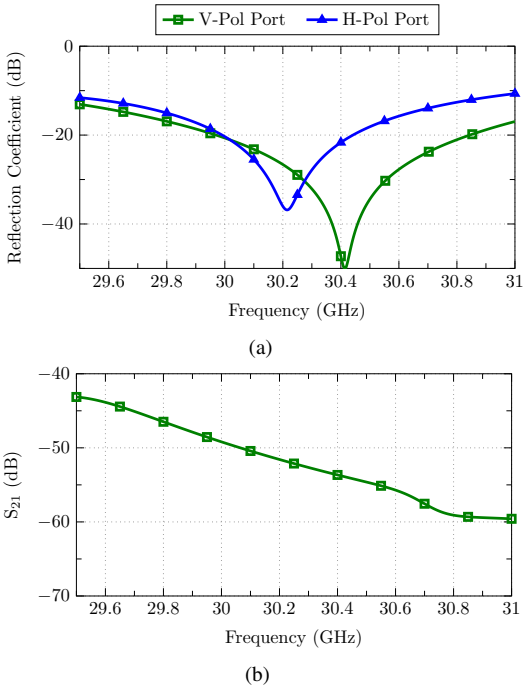

Fig. 7: S-parameters of the 2×2 dual-polarized unit cell.

top view. Cavities on each layer are fed corporately with orthogonal field components by Groove Gap Waveguides and Ridge Gap Waveguides (RGW) combined in the same feeding network. As demonstrated in [24], such network is an optimal approach to feed arrays in a symmetric and compact way.

Fig. 7 shows the S-parameters of the 2×2 array unit cell. The reflection coefficients (Fig. 7a) are not identical for both ports since conditions are not the same at both levels. Nonetheless, both return losses remains better than 10 dB within the targeted band, from 29.5 GHz to 31 GHz. Very good isolation between V-Pol and H-Pol layers is observed in Fig. 7b, partially thanks to the coupling slot between both cavities. Hence, S_{21}-parameter remains below -40 dB within the whole band.

It is worth mentioning that even though this type of feeding network has typically been used to feed uniform arrays, [23], [25], it could also be adjusted to feed tapered array distributions. A simple and useful strategy for that goal would be to modify the width and height in each RGW branch, RGW_A and RGW_B in Fig. 8a, which in turn will lead to unbalanced outputs. Additionally, the imbalance may be complemented by GGWs with different depth, i.e., different impedance. Fig. 8b, shows a comparison between the aperture field in the unit cell with and without uniform illumination. It should be stressed that, despite these modifications, the matching bandwidth remains similar to that of the uniform power distribution, as shown in Fig. 8c. The antenna presented here, though, is a proof of concept, not requiring any specific sidelobe level, thus a uniform array has been adopted for simplicity.

Regarding the radiating layer, a waffle grid is incorporated into the lid to increase the effective aperture area of the unit cell. As described in [23], an appropriate design of such grid

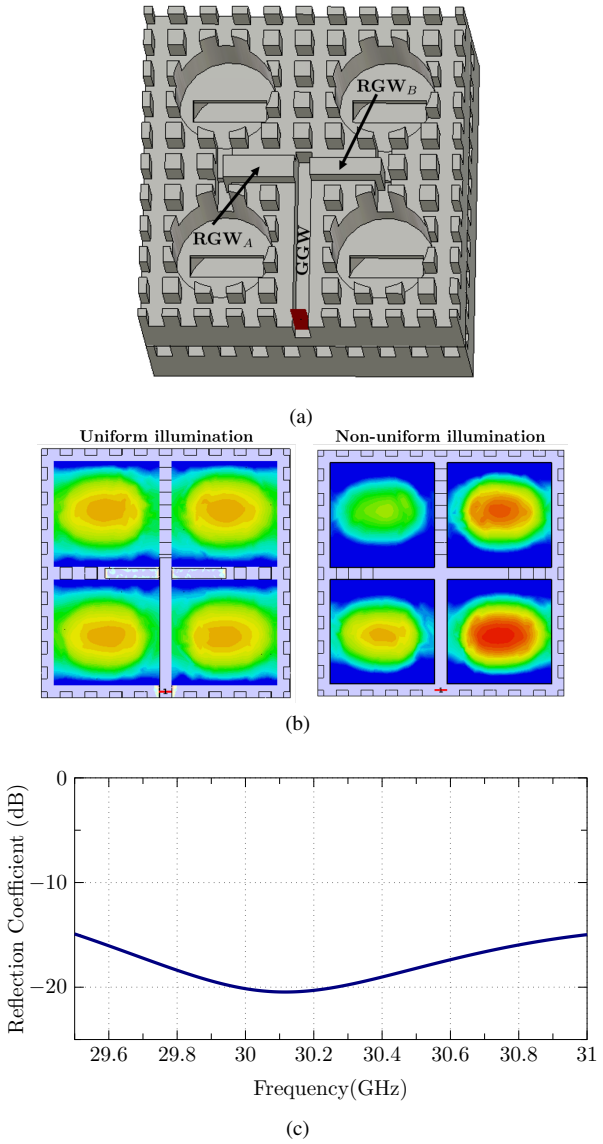

Fig. 8: (a) Cavities fed by an unbalanced power divider; (b) Field in the apertures using a balanced feeding (left) and an unbalanced one (right). (c) Reflection coefficient of the unit cell with the unbalanced feeding network.

TABLE I: Dimensions of the GGW in the corporate-feed network.

	Width (mm)	Height (mm)
GGW 1	1.75	2.61
GGW 2	1	2.57
GGW 3	1	2.57
GGW 4	1	2.67

alleviates the grating lobes issue when employing moderate spacings in arrays of apertures.

III. 8×8 Dual-Polarized Array Antenna

Once the geometry has been surveyed, the radiating element designed and the performance of the 2×2 dual-polarized unit cell demonstrated, the structure is extended to a larger array.

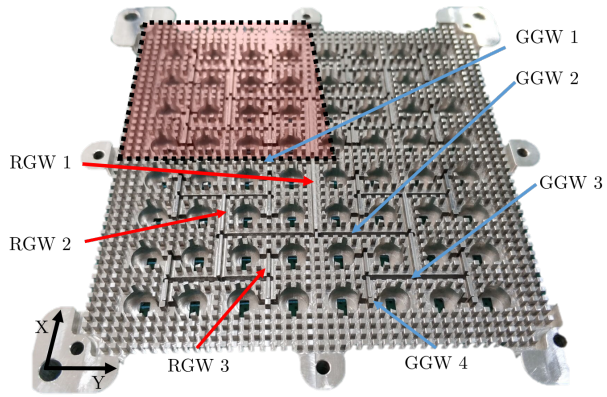

Fig. 9: Corporate feeding network for the 8×8 array. The full network is composed of 4 GGW and 3 RGW of different dimensions. By symmetry, the network is identical in each quadrant and at both levels.

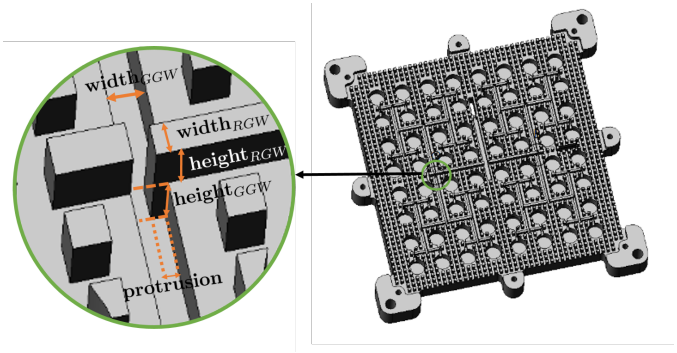

Fig. 10: Combined RGW-GGW divider. The fundamental parameters of each waveguide are indicated.

TABLE II: Dimensions of the RGW in the corporate-feed network.

	Width (mm)	Height (mm)	Protrusion (mm)
RGW 1	1	2.3	0.37
RGW 2	0.78	1.5	0.36
RGW 3	0.69	1.6	0.4

Fig. 9 shows one of the two feeding layers comprising the 8×8 array antenna. Nail height and width as well as periodicity are exactly the same for both layers. The diameter of the cavities and the dimensions of the corporate-feed distribution network are similar too. Fig. 9 illustrates that the full antenna consists of four identical quadrants (red square). The arrows indicate that three different RGW and four GGW sets can be found in the whole 1-to-64 corporate network. Waveguide dimensions are indicated in Tables I and II. Fig. 10 shows one of the RGW-GGW dividers of the network with the legend providing the most relevant parameters.

The input ports of both polarizations are located at the back side of the antenna, as shown in Figs. 11 and 12. Two transitions have been designed following the same strategy.

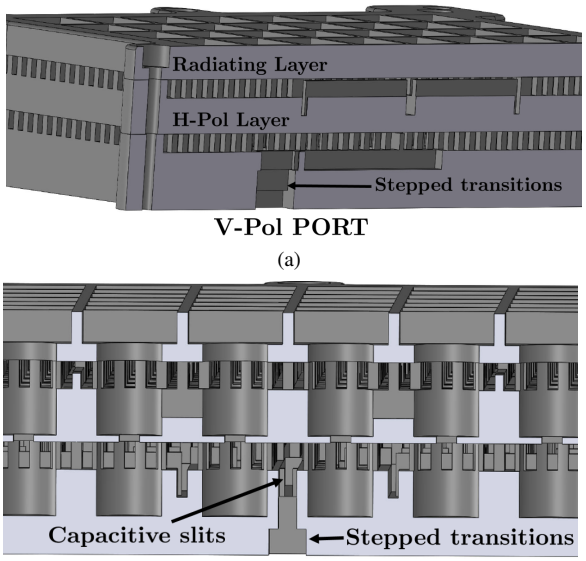

Fig. 11: Perspective and side view of the antenna showing the V-Pol transition.

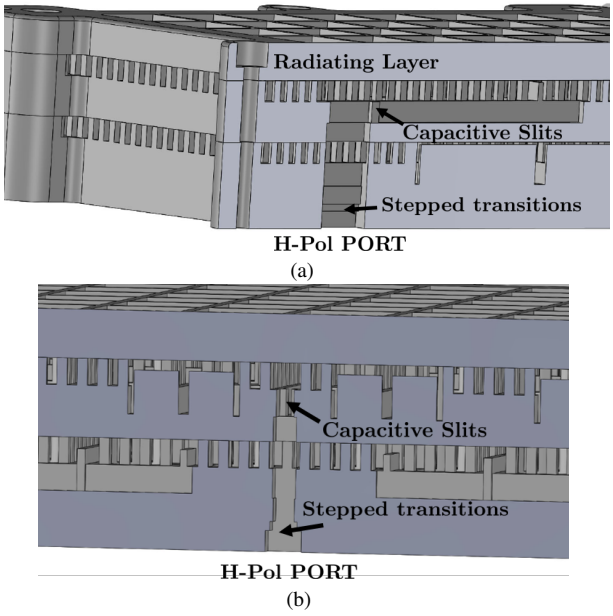

Fig. 12: Perspective and side view of the antenna showing the H-Pol transition.

A standard WR-28 input waveguide - whose dimensions are 7.112 mm×3.556 mm - must be adapted with a series of steps to the width of the first GGW shown in Table I. It should be noted that this groove is 75% wider than the rest of them, precisely to facilitate the matching from the back input port. At the beginning of the GGW 1 at each level, capacitive slits are located. They can be clearly seen in Figs. 11b and 12b. Both GGWs 1 in H-Pol and V-Pol layers include these slits to improve the impedance matching. Scattering parameters of the two input transitions were optimized separately and are shown in Fig. 13. The results demonstrate that the matching

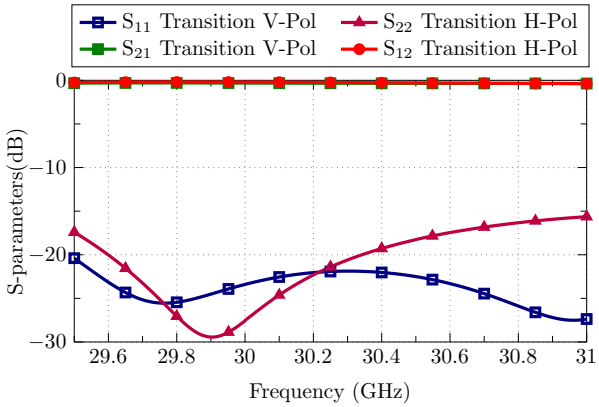

Fig. 13: Scattering parameters of the two input transitions.

performance for V-Pol transition is slightly better since it is structurally simpler. Note that H-Pol transition must pass through the V-Pol layer to access the GGW 1 at H-Pol layer.

Simulated results for the complete antenna are shown next. Fig. 14a exhibits that both S_{11}-parameters are below the target of -10 dB from 29.5 GHz to 31 GHz, which is a usual band for transmit in Ka-band SOTM applications. Fig. 14b demonstrates the isolation between ports. A decoupling level of more than 60 dB can be seen for the entire band of interest. Also, the simulated realized gain and ohmic losses within the bandwidth are included in Fig. 14c. Regarding the radiation patterns shown in Fig. 15, the XZ-plane cut for the V-Pol is almost equal to the YZ-plane cut for H-Pol and analogously for the other cuts. Good pattern shape and stability versus frequency can be noticed. In addition, the crosspolar components are shown too, being less than -50 dB in the whole band.

For the sake of completeness, let us mention that it would be possible to include a 90-degree hybrid coupler connected to both input ports so as to provide dual circular polarization. Just for illustration purposes, the H-pol port has been weighted with the same amplitude and a phase difference of 54° with respect to the V-Pol port. Notice that both transitions have different path lengths in such a way that, at the end, both layers will end up excited with the required 90° phase difference. Fig. 16 shows good polarization purity throughout the frequency range, obtaining an axial ratio below 0.6 dB. Besides, Fig. 17 shows the simulated normalized circularly-polarized radiation patterns.

IV. Experimental Results

The antenna described here has been fully manufactured in-house using a Datron M-25 CNC Milling Machine. Fig. 18 shows the three metallic pieces making up the whole antenna.

The manufacturing precision of the aluminum pieces was subjected to a metrology study. Fig. 19 illustrates a sample of some critical parts which are key for good antenna functioning. Circular ripples left by the milling cutter are visible (see purple circle in Fig. 19c). Such ripples, however, are merely one micron thick and their effect is negligible. In addition, a radius of curvature of 0.2 mm can be observed in the inner corners

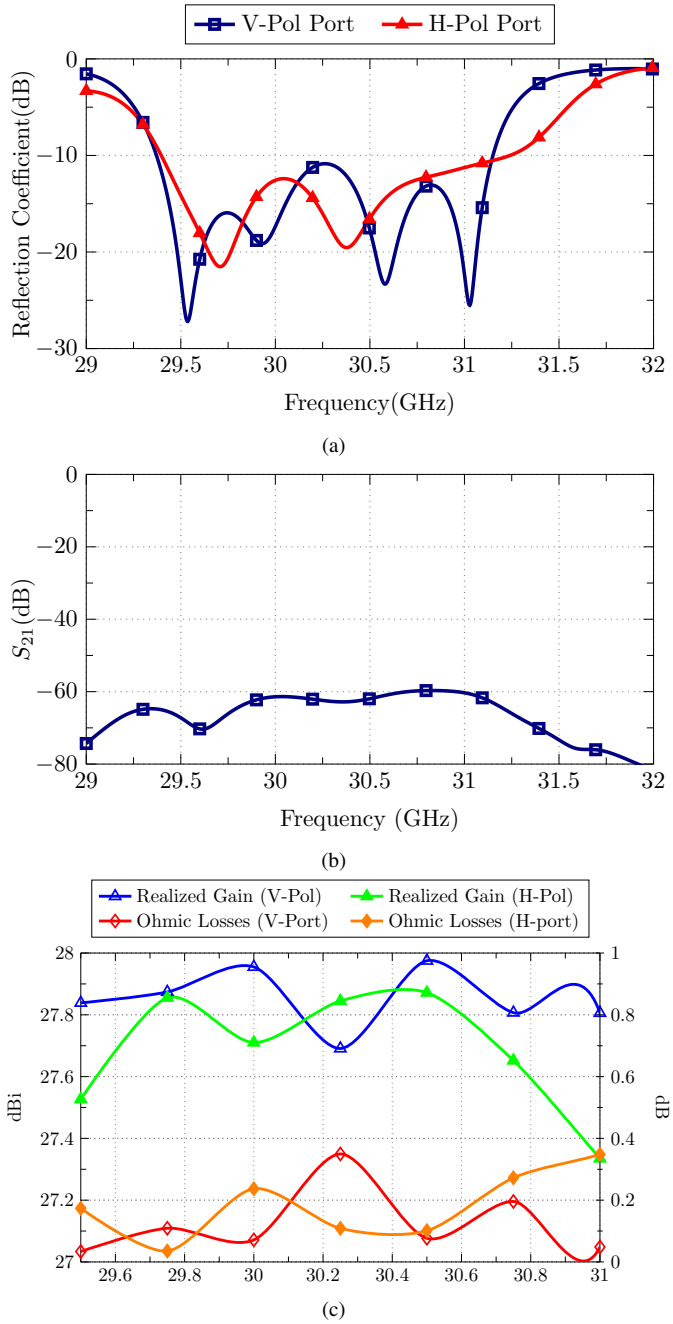

Fig. 14: Simulated S-parameters of the 8×8 Dual-Polarized Array Antenna: (a) S_{11} and S_{22}; (b) S_{21}; (c) Simulated realized gain and ohmic losses.

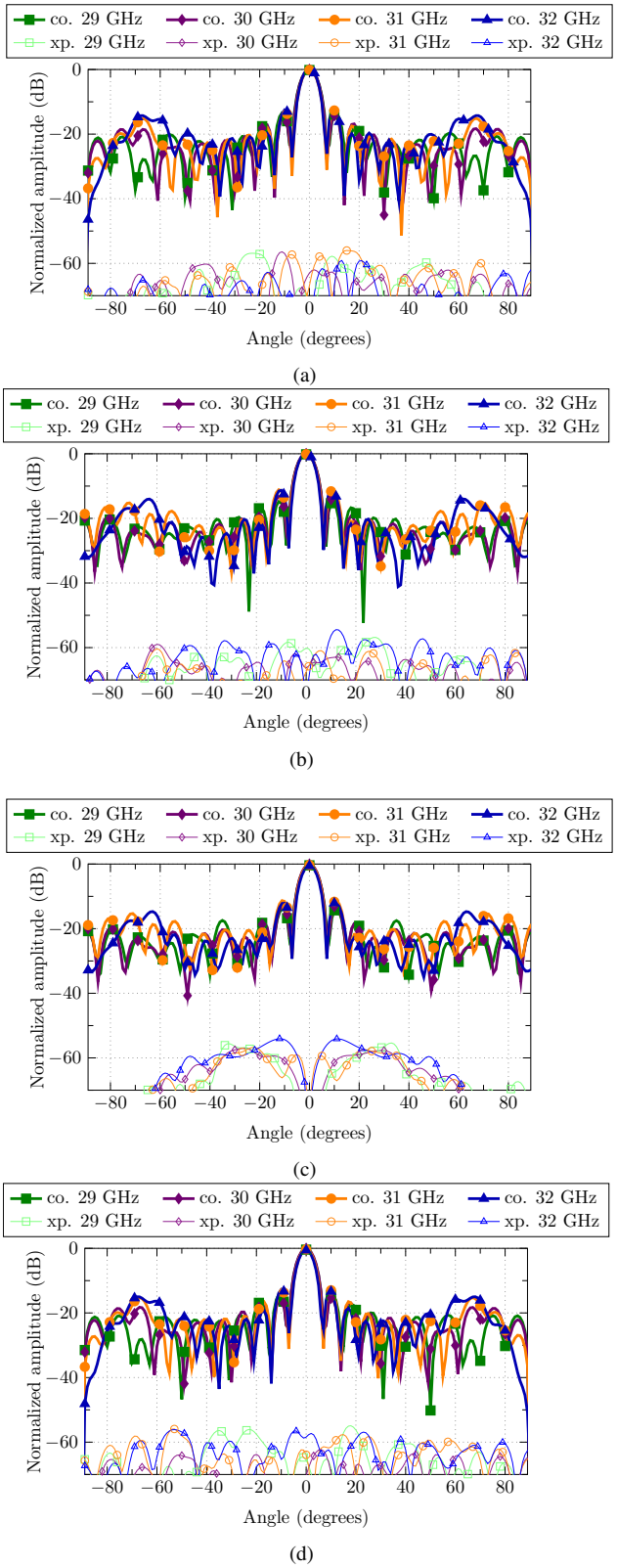

Fig. 15: Simulated normalized co-polar and cross-polar radiation patterns: (a) XZ-plane (V-Pol); (b) YZ-plane (V-Pol); (c) XZ-plane (H-Pol); (d) YZ-plane (H-Pol).

(see blue circles in Figs. 19a, 19b and 19d). This fact had already been taken into account in the simulated model.

The experimental validation of the manufactured prototype is observed in the following figures. Fig. 20a and Fig. 20b corresponds to V-Pol and H-Pol reflection coefficient, respectively. In these figures a comparison is made between simulation and measurement. Although the agreement is not perfect, curves show a similar behavior with a slight frequency shift, probably due to fabrication inaccuracies.

For V-Pol port, the reflection coefficient remains close to the goal of covering a 1.5-GHz bandwidth, though the curve is slightly above −10 dB around 30.5 GHz. Something similar occurs for H-Pol port, which holds a S_{11}-parameter below

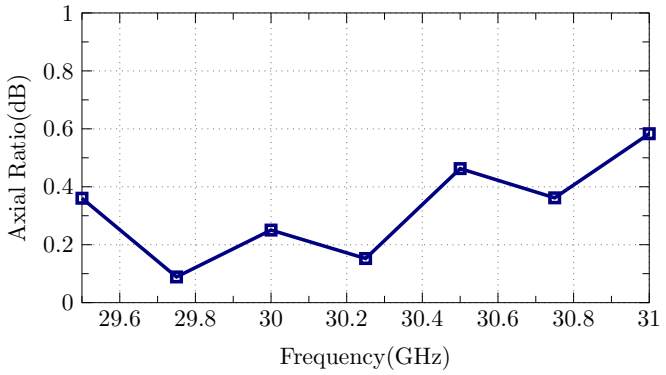

Fig. 16: Simulated axial ratio obtained using the proper phase excitation for the ports.

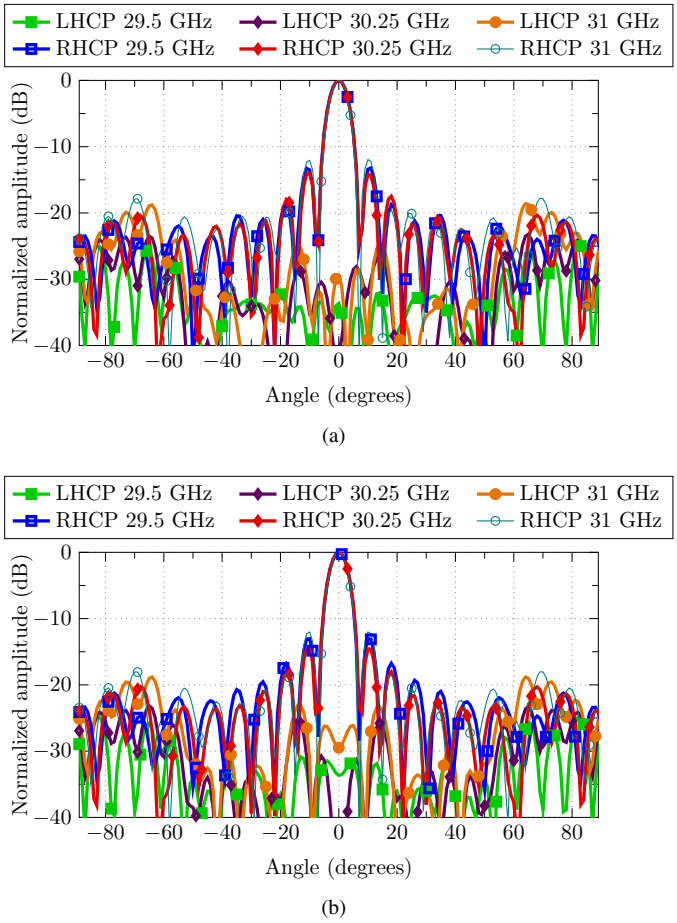

Fig. 17: Simulated normalized RHCP and LHCP radiation patterns obtained exciting ports with the proper phase for with circular polarization: (a) ϕ=0° and (b) ϕ=90°.

−10 dB from 29.8 GHz to 31.2 GHz. Also, a high level of isolation between ports is measured, being the S_{21}-parameter around −50 dB in the whole band (Fig. 20c).

The measured normalized co-polar and cross-polar radiation patterns are presented at several frequencies for both ports in Figs. 21 and 22. The results are highly satisfactory. Radiation patterns look fairly stable with frequency, very similar to those obtained in simulation. The mean measured realized gain

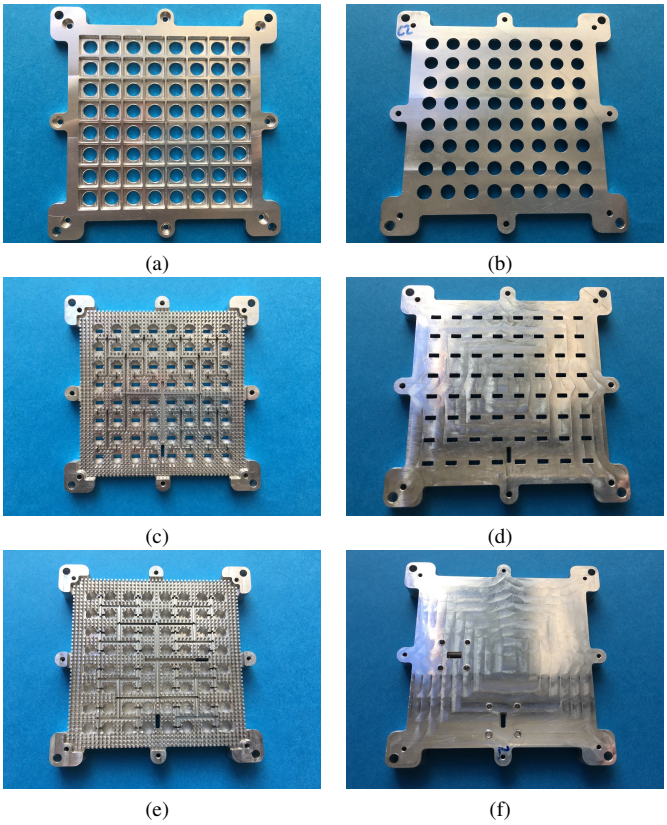

Fig. 18: The three manufactured aluminum pieces: (a) Front view and (b) back view of the radiating layer; (c) Front view and (d) back view of the V-Pol layer; (e) Front view and (f) back view of the H-Pol layer.

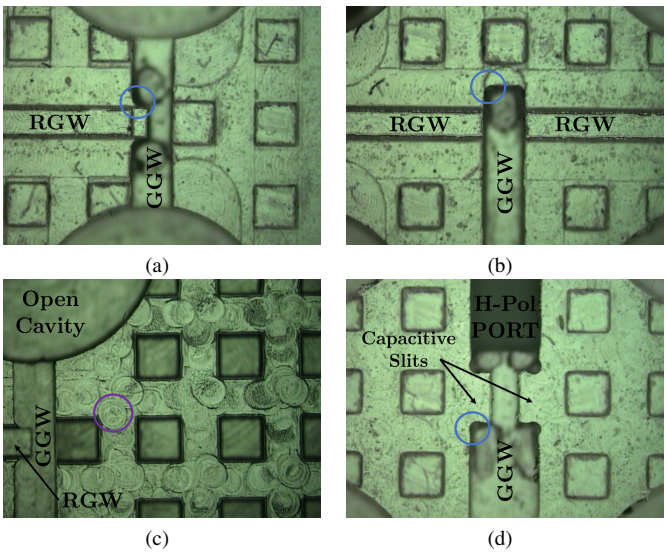

Fig. 19: Pictures of the metrology study to validate the manufacturing accuracy. (a) RGW to GGW divider. (b) GGW to RGW divider. (c) Bed of Nails. (d) H-Pol Port input transition.

within the bandwidth is over 27 dBi and the difference between gain and directivity is around 1 dB, revealing an antenna efficiency close to 80% over the entire bandwidth (Fig. 23).

The electric field on the aperture has been reconstructed

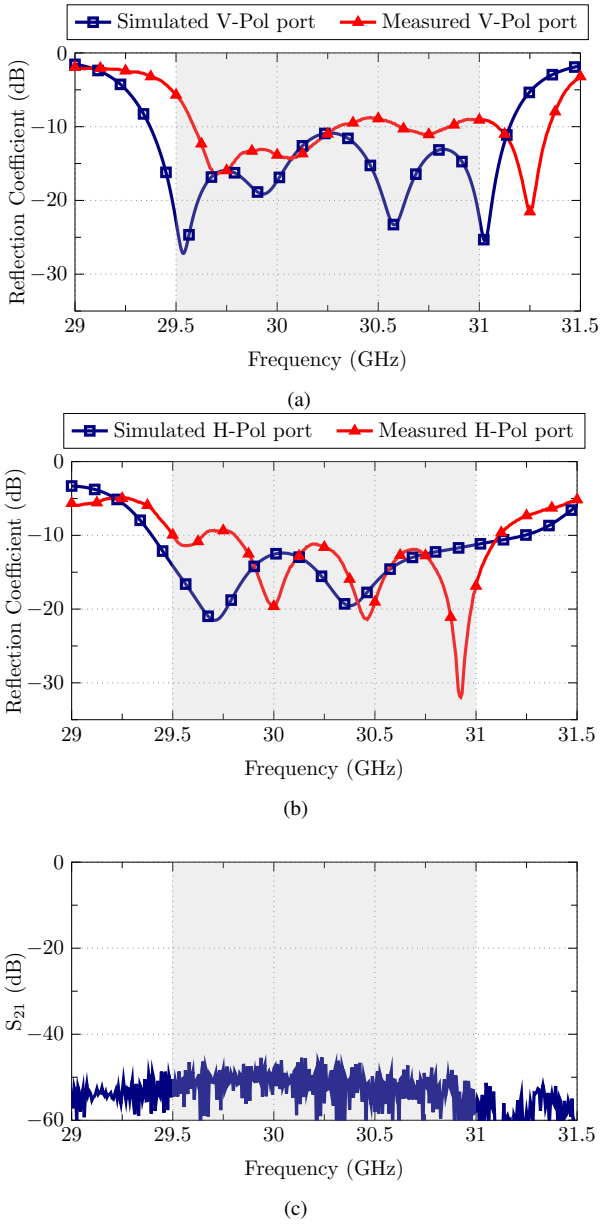

Fig. 20: Measured S-parameters of the dual-polarized array antenna. (a) Reflection coefficient of the V-Pol port. (b) Reflection coefficient of the H-Pol Port. (c) S_{21}.

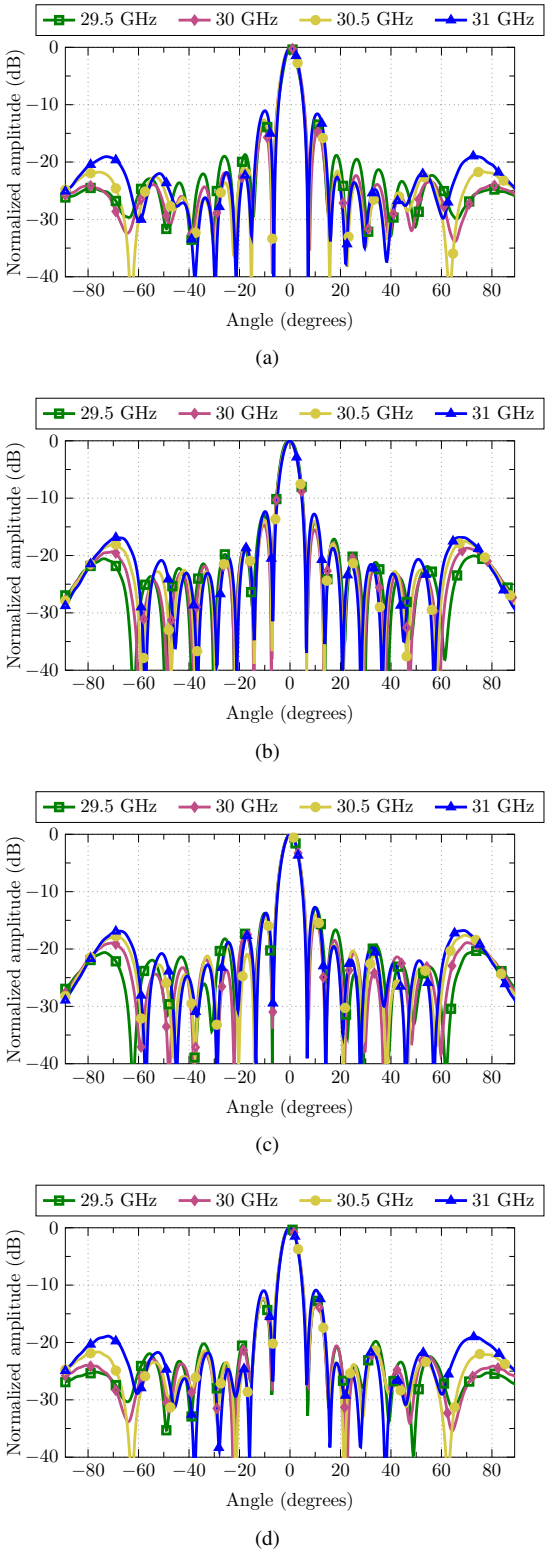

Fig. 21: Measured normalized co-polar radiation patterns: (a) XZ-plane (V-Pol); (b) YZ-plane (V-Pol); (c) XZ-plane (H-Pol); (d) YZ-plane (H-Pol).

from the far-field measurement at 30 GHz in Fig. 24. Good field uniformity throughout the array aperture is observed for both polarization. Finally, Fig. 25 shows a photograph of the antenna measurement set-up in the iTEAM-UPV facilities.

V. Conclusions

An 8×8 Ka-band dual linearly polarized array antenna using Gap Waveguide technology is presented. Circular apertures, backed by stacked cylindrical cavities, perform as radiating elements. Two feeding layers provide the desired dual-polarized performance, i.e. radiation of two orthogonal linear polarization when exciting two independent input ports.

The manufacturing process as well as the experimental validation has been detailed. Measurements present good agreement with simulation, revealing stable radiation patterns

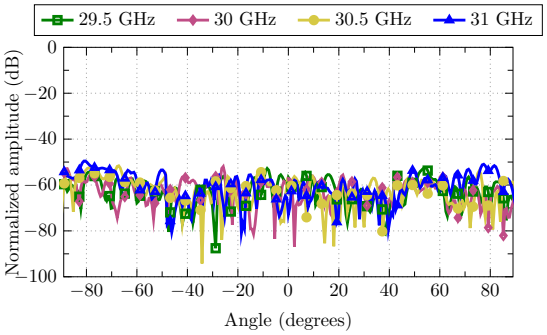

(a)

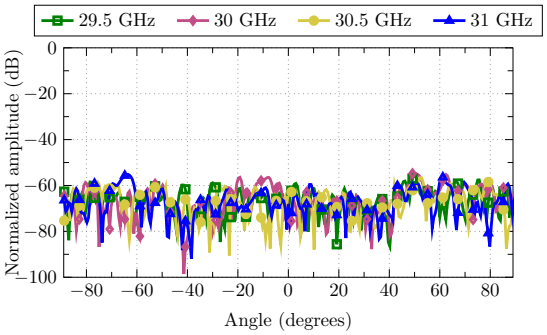

(b)

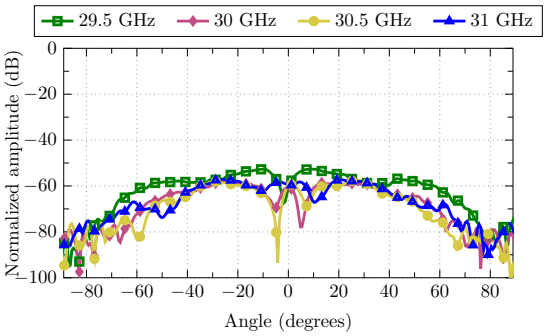

(c)

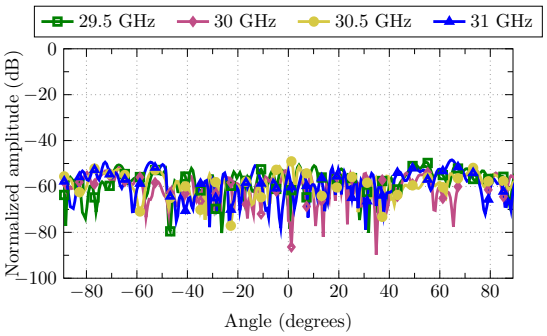

(d)

Fig. 22: Measured normalized cross-polar radiation patterns: (a) XZ-plane (V-Pol); (b) YZ-plane (V-Pol); (c) XZ-plane (H-Pol); (d) YZ-plane (H-Pol).

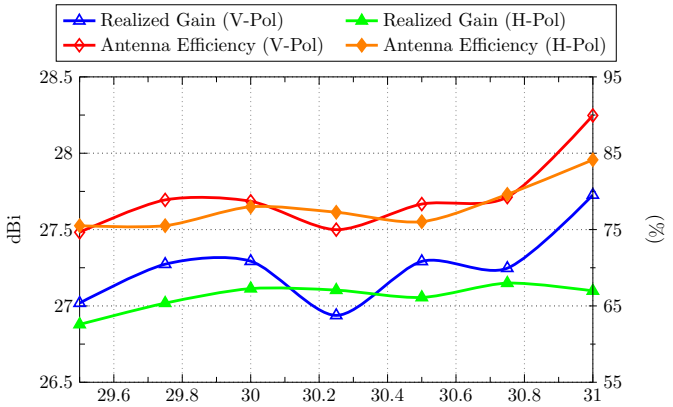

Fig. 23: Measured realized gain and antenna efficiency for both polarization.

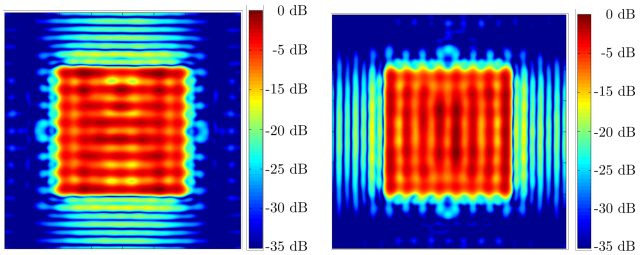

(a) (b)

Fig. 24: Aperture electric field, reconstructed from far field measurement at 30 GHz: (a) V-Pol; (b) H-Pol.

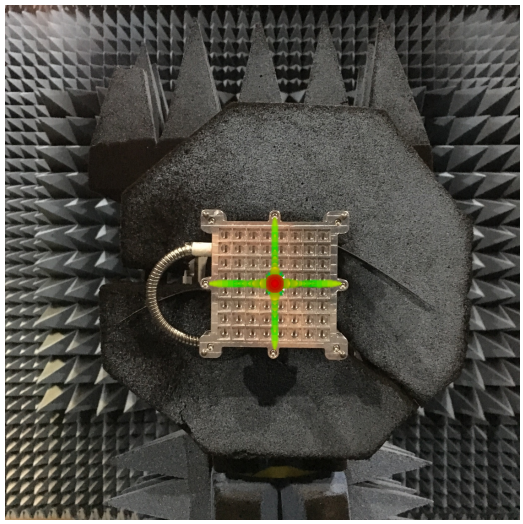

Fig. 25: Photograph of the antenna in the anechoic chamber. The 3D radiation pattern is superimposed.

for both polarization and high antenna efficiency, close to 80%.

The concept can be seamlessly extended to larger arrays without resorting to additional layers. Besides that, the extension to dual circular polarization, demanded for Ka-band SATCOM applications, can be easily achieved by the use of a 90-degree hybrid coupler, integrated into the lower part of the antenna.

To the best of the authors' knowledge, the presented work is the first dual-polarized antenna implemented in Gap Waveguide technology. Thanks to its efficiency, size, low profile and working band, this antenna can be an appealing solution for mechanical tracking systems in Satcom on-the-move applications.

VI. Acknowledgements

This work has been supported by the Spanish Ministry of Science, Innovation and Universities (Ministerio de Ciencia, Innovación y Universidades) under project TEC2016-79700-C2-1-R.

References

[1] B. Lesur, A. Maati, M. Thevenot, C. Menudier, E. Arnaud, T. Monediere, C. Melle, D. Chaimbault, and A. Karas, "A large antenna array for ka-band satcom-on-the-move applications-accurate modeling and experimental characterization," *IEEE Transactions on Antennas and Propagation*, vol. 66, no. 9, pp. 4586–4595, 2018.

[2] H. Fenech, S. Amos, A. Tomatis, and V. Soumpholphakdy, "High throughput satellite systems: An analytical approach," *IEEE Transactions on Aerospace and Electronic Systems*, vol. 51, no. 1, pp. 192–202, 2015.

[3] B. Ramamurth, W. G. Cowle, L. M. Davis, and G. Bolding, "Dual polarization frequency reuse in satcom: A method to counter poor cross-polar isolation," in *Military Communications Conference (MILCOM), 2014 IEEE*. IEEE, 2014, pp. 586–591.

[4] M. Veysi, M. Kamyab, and A. Jafargholi, "Single-feed dual-band dual-linearly-polarized proximity-coupled patch antenna," *IEEE Antennas and Propagation Magazine*, vol. 53, no. 1, pp. 90–96, 2011.

[5] N. V. Larsen and O. Breinbjerg, "An l-band, circularly polarized, dual-feed, cavity-backed annular slot antenna with wide-angle coverage," in *Proc. Int. Symp. IEEE Antennas and Propagation Society*, 2006, pp. 1549–1552.

[6] F. Mastrangeli, A. D. Luca, G. Valerio, and A. Galli, "Low-cost dual-polarized printed antenna for multifunction phased-array radar," *Microwave and Optical Technology Letters*, vol. 54, no. 3, pp. 697–702, 2012.

[7] Z. Liang, C. Lu, Y. Li, J. Liu, and Y. Long, "A broadband dual-polarized antenna with front-to-back ratio enhancement using semi-cylindrical sidewalls," *IEEE Transactions on Antennas and Propagation*, 2018.

[8] A. Mehrabani and L. Shafai, "Compact dual circularly polarized primary feeds for symmetric parabolic reflector antennas," *IEEE Antennas and Wireless Propagation Letters*, vol. 15, pp. 922–925, 2016.

[9] J. A. Encinar, L. S. Datashvili, J. A. Zornoza, M. Arrebola, M. Sierra-Castañer, J. L. Besada-Sanmartin, H. Baier, and H. Legay, "Dual-polarization dual-coverage reflectarray for space applications," *IEEE Transactions on Antennas and Propagation*, vol. 54, no. 10, pp. 2827–2837, 2006.

[10] E. Martinez-de Rioja, J. A. Encinar, M. Barba, R. Florencio, R. R. Boix, and V. Losada, "Dual polarized reflectarray transmit antenna for operation in ku-and ka-bands with independent feeds," *IEEE Transactions on Antennas and Propagation*, vol. 65, no. 6, pp. 3241–3246, 2017.

[11] C. Tienda, J. A. Encinar, M. Barba, and M. Arrebola, "Dual-polarization ku-band compact spaceborne antenna based on dual-reflectarray optics," *Sensors*, vol. 18, no. 4, p. 1100, 2018.

[12] D. Sanchez-Escuderos, M. Ferrando-Rocher, J. I. Herranz-Herruzo, H. C. Moy-li, and A. Valero-Nogueira, "Dual-polarized frequency selective surface for sotm applications," in *Antennas and Propagation (EUCAP), 2018 12th European Conference on*. IEEE, 2018.

[13] T. Jaschke, H. K. Mitto, and A. F. Jacob, "K/ka-band dual-polarized siw-fed lens antennas for rx/tx integration," *International Journal of Microwave and Wireless Technologies*, pp. 1–8, 2018.

[14] D. Kim, M. Zhang, J. Hirokawa, and M. Ando, "Design and fabrication of a dual-polarization waveguide slot array antenna with high isolation and high antenna efficiency for the 60 ghz band," *IEEE Transactions on Antennas and Propagation*, vol. 62, no. 6, pp. 3019–3027, 2014.

[15] I. Nistal-González, S. Otto, O. Litschke, A. Bettray, L. Wunderlich, R. Gieron, and M. Wleklinski, "Planar phased array antenna for nomadic satellite communication in ka-band," in *Microwave Conference (EuMC), 2014 44th European*. IEEE, 2014, pp. 1699–1702.

[16] C.-X. Mao, S. Gao, Q. Luo, T. Rommel, and Q.-X. Chu, "Low-cost x/ku/ka-band dual-polarized array with shared aperture," *IEEE Trans. Antennas Propag.*, vol. 65, no. 7, pp. 3520–3527, 2017.

[17] O. Yurduseven, N. L. Juan, and A. Neto, "A dual-polarized leaky lens antenna for wideband focal plane arrays," *IEEE Transactions on Antennas and Propagation*, vol. 64, no. 8, pp. 3330–3337, 2016.

[18] M. Ferrando-Rocher, A. Valero-Nogueira, J. I. Herranz-Herruzo, A. Berenguer, and B. Bernardo-Clemente, "Groove gap waveguides: A contactless solution for multilayer slotted-waveguide array antenna assembly," in *Antennas and Propagation (EuCAP), 2016 10th European Conference on*. IEEE, 2016, pp. 1–4.

[19] A. U. Zaman and P.-S. Kildal, "Gap waveguides," in *Handbook of Antenna Technologies*. Springer, 2016, pp. 3273–3347.

[20] D. Zarifi, A. Farahbakhsh, A. U. Zaman, and P.-S. Kildal, "Design and fabrication of a high-gain 60-ghz corrugated slot antenna array with ridge gap waveguide distribution layer," *IEEE Transactions on Antennas and Propagation*, vol. 64, no. 7, pp. 2905–2913, 2016.

[21] A. Farahbakhsh, D. Zarifi, and A. U. Zaman, "60-ghz groove gap waveguide based wideband h-plane power dividers and transitions: For use in high-gain slot array antenna," *IEEE Transactions on Microwave Theory and Techniques*, vol. 65, no. 11, pp. 4111–4121, 2017.

[22] M. Ferrando-Rocher, A. Zaman, J. Yang, and A. Valero-Nogueira, "A dual-polarized slotted-waveguide antenna based on gap waveguide technology," in *Antennas and Propagation (EUCAP), 2017 11th European Conference on*. IEEE, 2017, pp. 3726–3727.

[23] M. Ferrando-Rocher, J. I. Herranz-Herruzo, A. Valero-Nogueira, and A. Vila-Jiménez, "Single-layer circularly-polarized ka-band antenna using gap waveguide technology," *IEEE Transactions on Antennas and Propagation*, 2018.

[24] M. Ferrando-Rocher, A. Valero-Nogueira, and J. I. Herranz-Herruzo, "New feeding network topologies for high-gain single-layer slot array antennas using gap waveguide concept," in *Antennas and Propagation (EUCAP), 2017 11th European Conference on*. IEEE, 2017, pp. 1654–1657.

[25] M. Ferrando-Rocher, J. I. Herranz, A. Valero-Nogueira, and B. Bernardo, "Performance assessment of gap waveguide array antennas: Cnc milling vs. 3d printing," *IEEE Antennas and Wireless Propagation Letters*, 2018.

Miguel Ferrando-Rocher (S'15) was born in Alcoy, Spain. He received the M.Sc. and Ph.D. degrees in telecommunication engineering from the Universitat Politcnica de Valncia (UPV), Valencia, Spain, in 2012 and 2018, respectively. In 2012, he joined the Complex Radiation Systems Team, Institute of Electronics and Telecommunications Rennes, Rennes, France, as a Researcher, where he was involved in reflectarray antennas for satellite applications in collaboration with Thales Alenia Space. Since 2013, he has been with the Electromagnetic Radiation Group, Institute of Telecommunications and Multimedia Applications, UPV. In 2016, he was a Guest Researcher with the Chalmers University of Technology, Gothenburg, Sweden. He received an Erasmus grant to study at Ghent University, Ghent, Belgium, in 2010. His current research interests include satellite communications on-the-move, highgain antennas and arrays, gap waveguide technology, and millimeter-wave components. Dr. Ferrando-Rocher was a recipient of the URSI Conference Best Student Paper Award in 2017 and the Jury Prize and the Audience Prize to the best oral presentation of the II Meeting of Ph.D. Students at UPV.

José Ignacio Herranz Herruzo was born in Valencia, Spain, in 1978. He received the degree in telecommunication engineering from the Universitat Politècnica de Valencia, Valencia, Spain, in 2002. He is currently pursuing the Ph.D. degree. He joined the Departamento de Comunicaciones, Universitat Politécnica de Valencia, in 2002, where he is currently working as an Assistant Professor. His research interests include optimization of waveguide slot array antennas and efficient computational methods for planar structures.

Alejandro Valero-Nogueira (S'92-M'97-SM'09) was born in Madrid, Spain, on July 19, 1965. He received the degree in telecommunication engineering from the Universidad Politècnica de Madrid, Madrid, Spain, and the Ph.D. degree in telecommunication from the Universitat Politècnica de Valencia, Valencia, Spain, in 1991 and 1997, respectively. In 1992, he joined the Departamento de Comunicaciones, Universitat Politècnica de Valencia, where he is currently an Associate Professor. During 1999, he was on leave at the ElectroScience Laboratory, The Ohio State University, Columbus, OH, USA, where he was involved in fast solution methods in electromagnetics and conformal antenna arrays. His research interests include computational electromagnetics, waveguide slot arrays, gap waveguides, the theory of characteristic modes, and automated antenna design procedures.

Bernardo Bernardo-Clemente was born in Valencia, Spain, on May 8, 1972. He received the degree in telecommunication engineering from Univeritat Politècnica de València in 2003. He is currently working toward the Ph. D. degree in telecommunication. He has been with the Institute of Telecommunicactions and Multimedia Applications (ITEAM) since 2005. His main research interests include antenna measurement, antenna fabrication, near to far field transformation.

Ashraf Uz-Zaman (M'14) was born in Chittagong, Bangladesh. He received the B.Sc. degree from the Chittagong University of Engineering and Technology, Chittagong, and the M.Sc. and Ph.D. degrees from the Chalmers University of Technology, Gothenburg, Sweden, in 2007 and 2013, respectively. He is currently an Assistant Professor with the Communication and Antenna Division, Chalmers University of Technology. His current research interests include millimeter-wave high-efficiency planar antennas, gap waveguide technology, frequency-selective surfaces, microwave passive components, and packaging techniques and integration of MMICs with the antennas.

Jian Yang (M'01 - SM'10) received the B.Sc. degree in electrical engineering from the Nanjing University of Science and Technology, Nanjing, China, in 1982, the M.Sc. degree in electrical engineering from the Nanjing Research Center of Electronic Engineering, Nanjing, in 1985, and the Swedish Licentiate and Ph.D. degrees from the Chalmers University of Technology, Gothenburg, Sweden, in 1998 and 2001, respectively. From 1985 to 1996, he was a Senior Engineer with the Nanjing Research Institute of Electronics Technology, Nanjing. From 1999 to 2005, he was a Research Engineer with the Department of Electromagnetics, Chalmers University of Technology, Gothenburg, Sweden. From 2005 to 2006, he was a Senior Engineer with COMHAT AB. From 2006 to 2010, he was an Assistant Professor with the Chalmers University of Technology. From 2010 to 2016, he was an Associate Professor with the Department of Signals and Systems, Chalmers University of Technology. Since 2016, he has been a Professor with the Department of Electrical Engineering, Chalmers University of Technology. He has authored and co-authored about 60 journal articles and about 150 conference papers. He holds more than 10 granted patents. His current research interests include 60140 GHz antennas, terahertz antennas, MIMO antennas, ultrawideband (UWB) antennas and UWB feeds for reflector antennas, UWB radar systems, UWB antennas in near-field sensing applications, hat-fed antennas, reflector antennas, radome design, and computational electromagnetics.